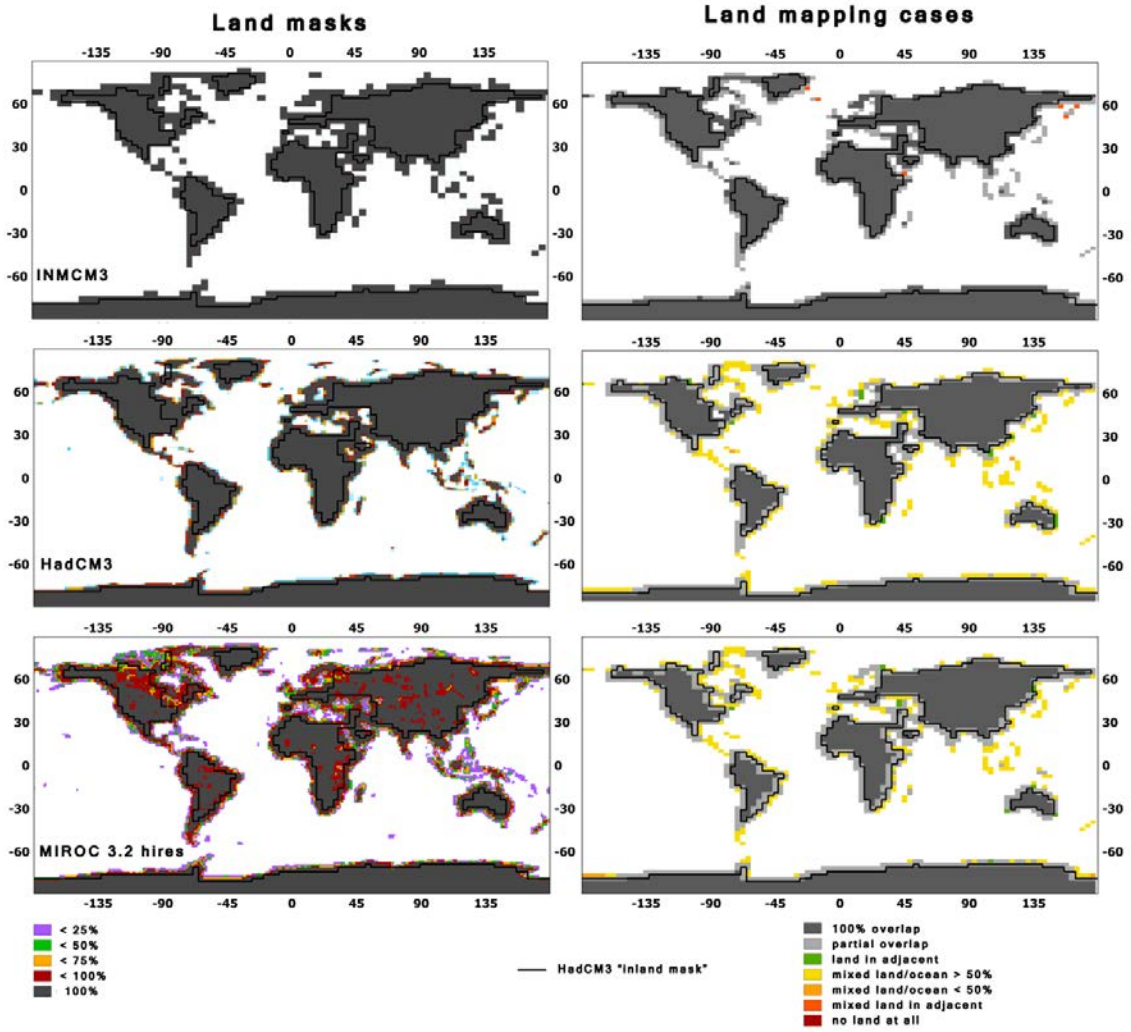

Figure S1. Three examples of GCM grids (on the left), representing main grid categories in the CMIP3 dataset. Diagrams on the right show where different re-gridding strategies were applied in order to translate each grid-box into the UKMO-HadCM3 GCM land grid-boxes.

5

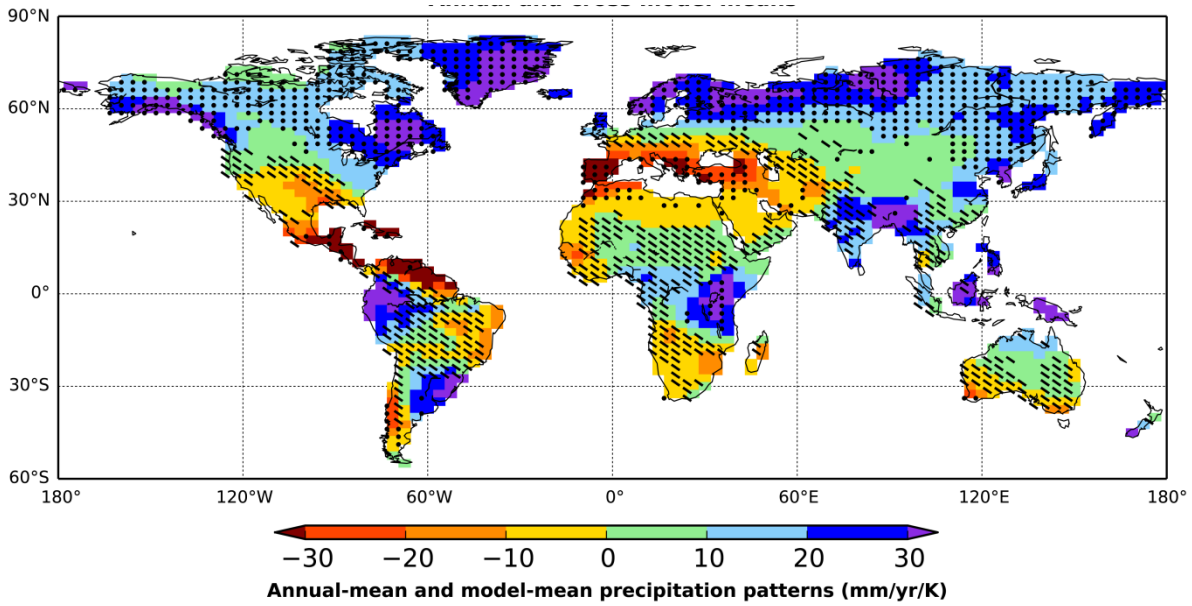

5

Figure S2. Annual means and variation (2*SD) in the monthly patterns of local precipitation change per degree warming over all land (mm yr-1 K-1), across 22 GCMs. In regions marked with stippling more than 66% of the models agree in the sign of the change. This figure has been prepared to enable comparison with Figure 10.9 in Meehl et al (2007).

Table S1. Type of overlap between land grid-boxes of the UKMO-HadCM3 grid and corresponding areas across other 22 GCM considered in this study.

	Mapping case	Number of cases	Fraction of the dataset
1	only 100% land overlaid and averaged	32900	0.6281
2	some 100% land overlaid and averaged (ocean and mixed areas)	14012	0.2675
3	100% land found in the neighbourhood and 100% land cases averaged	119	0.0023
4	no 100% land in the neighbourhood found, so take mixed land (frac>=0.5) from the grid-box	5109	0.0975
5	no 100% land in the neighbourhood found, so take mixed land (frac>0) from the grid-box	183	0.0035
6	no 100% land in the neighbourhood found, nor mixed land in the grid-box, but mixed land in the neighbourhood	6	0.0001
7	no land at all found (so simple averaging done)	53	0.0010

Supplementary Material

S1. Files containing climate change patterns

The final climate pattern scaling set is available in two versions: A: with precipitation normalised (file pattRelPrFin_v3c.zip, see Data and Methods), and B: without normalisation (file pattFin_v3c.zip).

Each of the two dataset versions contains 22 directories with named after GCMs considered in this study (pattRelPR_d2_GCMNAME and patt_d2_GCMNAME in version A and B, respectively). Each directory contains 12 ASCII text files with names corresponding to months they represent. Each file contains a one-line header followed by 1631 lines, each one containing patterns for a single location. Meaning of consecutive columns is as follows:

1. Longitude, 2. Latitude, 3. TAS pattern, 4. HUR at surface pattern, 5. Wind (UAS+VAS) pattern, 6. (empty), 7. RLDS pattern, 8. RSDS pattern, 9. (empty), 10. PR pattern, 11. PRSN, 12. PS pattern, 13. (empty)

IMOGEN EBM calibration parameters are given in Table 2.

The files can be downloaded at:

S2. Homogenisation of GCM resolutions and land masks

ESMs differ between each other in terms of how precisely they represent the Earth surface's detail (as represented in the "land mask" variable SFTLF). Spatial resolution of these data varies between ESMs (Table 1), ranging from hundreds of kilometres (e.g. GISS models, or INM-CM3.0) to around 50 km (e.g. MIROC3.2hires). Concerning grid spacing, data are mapped on either a regular or a Gaussian grid. In addition, ESM grid-boxes are split into land and water in a number of ways (see below). This diversity of output spatial properties alone imposes a challenge for data end-users, including policymakers.

Implementation of CMIP3 patterns in the IMOGEN system included transforming all types of WCRP CMIP3 grids into one, which was chosen to be the UKMO-HadCM3, based on the need for compatibility with previous applications of the tool.

There are four types of land mask: (i) binary (each grid box is100% land, or 100% water, e.g. UKMO-HadCM3), (ii) continuous without inland waters (from 0% to 100% of land, e.g. UKMO-HadGEM1), (iii) binary for oceans, continuous for inland waters (e.g. GISS models), (iv) continuous with inland waters (MIROC3.2(hires)). This is important because the IMOGEN tool was originally designed to model impact over land (excluding Antarctica), assuming different warming rate for land and ocean areas, and therefore the climate patterns used to drive it need to apply to land as much as possible. In order to achieve that, the following procedure was implemented.

First, spatial resolution of CMIP3 data was homogenized to 1 x 1 degree through bilinear interpolation. Subsequently, the data were re-mapped onto the HadCM3 model grid with binary representation of land and ocean and no inland freshwater

bodies. The mapping procedure distinguishes between land, ocean and mixed areas, and allows for minor spatial shifts in grid boxes in order to preserve the land/ocean contrast in surface variables. Since the initial 1 x 1degree resolution is finer than in the HadCM3 grid, this enables the procedure of segregation of fine grid-boxes overlapping with a particular HadCM3 land grid-box, according to the proportion of land they represent. When '100%' land fine grid-boxes are present, only these are averaged and assigned the HadCM3 grid-box. Fractional land grid-boxes are used in the absence of 100% land and in the rare cases when no land overlaps with the HadCM3 land grid-box then the immediate neighbourhood is included in the procedure. Land areas represented in the final output may exhibit a significantly altered behaviour (in terms of mean surface temperature and Top-Of-Atmosphere radiative fluxes); however, this dataset is only used to characterise 'pure' land occurring within, or nearby, each grid-box, while the assessment of global changes in temperature, or modelling of the energy balance of land and ocean is done using AOGCM data in its original format.

Relationship between the radiative forcing due to CO_2 increase and the surface temperature increase over land and ocean is derived based on the original GCM data, before its mapping onto UKMO-HadCM3 grid. It relies on the decoupling of energy fluxes over land and oceans, which in the 'continuous' grids is hampered into a small extent because of the existence of grid-boxes containing both land and ocean, where partitioning of energy fluxes between land and ocean with full certainty is not possible. In the case of a few grids which represent inland fresh water, the UKMO-HadCM3 representation of inland was used to over-write the original land fraction values.

S3. Trends in annual precipitation change - comparison with IPCC data

References (Supplementary Material)

Cox, P. M., Betts, R. A., Collins, M., Harris, P. P., Huntingford, C. and Jones, C.D.: Amazonian forest dieback under climate-carbon cycle projections for the 21st century, Theor. Appl. Climatol., 78, 137-156, doi:10.1007/s00704-004-0049-4, 2004.

Cox, P. M., Betts, R. A., Jones, C. D., Spall, S. A. and Totterdell, I. J.: Acceleration of global warming due to carbon-cycle feedbacks in a coupled climate model, Nature, 408, 184-187, doi:10.1038/35041539, 2000.

Hughes, J. K., Lloyd, A. J., Huntingford, C., Finch, J. W. and Harding, R. J.: The impact of extensive planting of Miscanthus as an energy crop on future CO2 atmospheric concentrations, Glob. Change Biol. Bioenergy, 2, 79-88, doi:10.1111/j.1757-1707.2010.01042.x, 2010.

Huntingford, C., Booth, B. B. B., Sitch, S., Gedney, N., Lowe, J. A., Liddicoat, S. K., Mercado, L. M., Best, M. J., Weedon, G. P., Fisher, R. A., Lomas, M. R., Good, P., Zelazowski, P., Everitt, A. C., Spessa, A. C., Jones, C. D.: IMOGEN: an intermediate complexity model to evaluate terrestrial impacts of a changing climate, Geosci. Model Dev., 3, 679-687, doi:10.5194/gmd-3-679-2010, 2010.

Huntingford, C. and Cox, P. M.: An analogue model to derive additional climate change scenarios from existing GCM simulations, Clim. Dynam., 16, 575-586, doi:10.1007/s003820000067, 2000.

Huntingford, C., Cox, P. M., Mercado, L. M., Sitch, S., Bellouin, N., Boucher, O. and Gedney, N.: Highly contrasting effects of different climate forcing agents on terrestrial ecosystem services, Philos. T. R. Soc. A, 369, 2026-2037, doi:10.1098/rsta.2010.0314, 2011.

Huntingford, C., Smith, D. M., Davies, W. J., Falk, R., Sitch, S. and Mercado, L.M..: Combining the ABA and net photosynthesis-based model equations of stomatal conductance, Ecol. Model., 300, 81-88, doi:10.1016/j.ecolmodel.2015.01.005, 2015.

IPCC: The Physical Science Basis. Contribution of Working Group I to the Fifth Assessment Report on the Intergovernmental Panel on Climate Change, Cambridge University Press, Cambridge, United Kingdom and New York, New York, United States of America, 1535 pp., 2013.

Mercado, L. M., Bellouin, N., Sitch, S., Boucher, O., Huntingford, C., Wild, M. and Cox, P. M.: Impact of changes in diffuse radiation on the global land carbon sink, Nature, 458, 1014-U87, doi:10.1038/nature07949, 2009.

Meehl, G. A., T. F. Stocker, W. D. Collins, P. Friedlingstein, A. T. Gaye, J. M. Gregory, A. Kitoh, R. Knutti, J. M. Murphy, A. Noda, S. C. B. Raper, I. G. Watterson, A. J. Weaver and Z.-C. Zhao: Global Climate Projections. In: Climate Change 2007: The Physical Science Basis. Contribution of Working Group I to the Fourth Assessment Report of the Intergovernmental Panel on Climate Change [Solomon, S., D. Qin, M. Manning, Z. Chen, M. Marquis, K. B. Averyt, M. Tignor and H. L. Miller (eds.)], Cambridge University Press, Cambridge, United Kingdom and New York, NY, USA., 2007.

Sitch, S., Cox, P. M., Collins, W. J. and Huntingford, C.: Indirect radiative forcing of climate change through ozone effects on the land-carbon sink, Nature, 448, 791-U4, doi:10.1038/nature06059, 2007.

Sitch, S., Huntingford, C., Gedney, N., Levy, P. E., Lomas, M., Piao, S. L., Betts, R., Ciais, P., Cox, P., Friedlingstein, P., Jones, C. D., Prentice, I. C. and Woodward, F. I.: Evaluation of the terrestrial carbon cycle, future plant geography and climate-carbon cycle feedbacks using five Dynamic Global Vegetation Models (DGVMs), Glob. Change Biol., 14, 2015-2039, doi: 10.1111/j.1365-2486.2008.01626.x, 2008.